Identification of Two-Mass Mechanical Systems Using Torque Excitation: Design and Experimental Evaluation

Seppo E. Saarakkala and Marko Hinkkanen, *Senior Member, IEEE*

Abstract—This paper deals with methods for parameter estimation of two-mass mechanical systems in electric drives. Estimates of mechanical parameters are needed in the start-up of a drive for automatic tuning of model-based speed and position controllers. A discrete-time output error (OE) model is applied to parameter estimation. The resulting pulse-transfer function is transformed into a continuous-time transfer function, and parameters of the two-mass system model are analytically solved from the coefficients of this transfer function. An open-loop identification setup and two closed-speed-loop identification setups (direct and indirect) are designed and experimentally compared. The experiments are carried out at nonzero speed to reduce the effect of nonlinear friction phenomena on the parameter estimates. According to results, all three identification setups are applicable for the parameter estimation of two-mass mechanical systems.

Index Terms—Electric drives, parameter estimation, resonant mechanical load, torsional oscillation.

I. INTRODUCTION

HIGH-PERFORMANCE ac electric drives are replacing pneumatic and hydraulic actuators or dc motor drives in modern machineries—such as injection molding machines [1], machine tools [2], industrial robots [3]—due to their energy efficiency, compact size, and flexible control algorithms. These machineries often consist of several moving or rotating masses coupled together with flexible mechanical transmissions (e.g., belts, gearboxes, long shafts), leading to mechanical resonances. To achieve high dynamic performance, motion control of the drive systems with resonant mechanical loads should be based on higher-order mechanical models. The model-based automatic controller tuning typically relies on the knowledge of mechanical parameters and some performance specifications (e.g., closed-loop bandwidth) [4], [5]. However, datasheets of the mechanical components are not often available or the calculation of the mechanical parameters can be a highly complex

task. Hence, to enable model-based automatic tuning of the motion controllers, the mechanical parameters should be automatically identified during the start-up of a drive [6], [7] or online during the drive operation [8]–[12]. The extended Kalman filter is a popular tool for estimating the parameters online [8], [10], [11]. However, the main difficulty with the Kalman filters is the selection of covariance matrices, which are further needed when calculating the filter coefficients. Moreover, it is worth mentioning that the identification of the mechanical system may offer a possibility to diagnose mechanical faults. As examples, a rolling-bearing damage [13] and gearbox faults [14], [15] can be identified using electric drives.

The identification routines, proposed for parameter estimation of two- or multi-mass mechanical systems, can be roughly divided to parametric methods [3], [6], [16]–[20] and nonparametric methods [16], [21]–[24]. The nonparametric methods use the frequency-domain characteristics of the system, while, in the parametric methods, the parameters of the two-mass system transfer-function polynomials are estimated in the time domain. When the identification is completed offline, e.g., during the start-up of a drive, the parameters of the mechanical model can be estimated either in open loop or using closed-loop speed control [25]. It is desirable to reduce the effect of nonlinear friction phenomena on parameter estimates by operating at nonzero speed. However, when using the open-loop method, it may be difficult to find a suitable value for the offset torque without causing the system to rush. On the other hand, in closed-loop identification, the drive can be easily operated at desired (nonzero) speed. Closed-loop identification methods can be divided into direct and indirect methods [25]. In the case of direct methods, the input signal is affected via the feedback loop. Hence, a correct noise model is needed. In the case of indirect methods, the closed-loop system is first identified, and the open-loop model is then solved using the known control law [26].

To excite the identified system sufficiently, the excitation signal should contain all frequencies evenly distributed, and the amplitude of the excitation signal should be as large as possible. White noise is normally utilized in stochastical identification. In electric drives, the torque and the speed are limited to their maximum allowed values. With limited input signals, the largest frequency variation is obtained by binary signals, which have only two possible values (e.g., -1 and 1). A pseudorandom binary signal (PRBS) fulfills the previously stated requirements, and it can be easily formed with a shift register. The statistical properties of the PRBS are studied in [27].

In this paper, the mechanical system is excited using the PRBS, which is superimposed on the electromagnetic torque by means of field-oriented control. The rotor-speed response of the driving motor is measured. Because the rotor-speed response is noisy, the discrete-time OE model is used in identification, in accordance with [3]. The main contributions of this paper are:

1) An indirect closed-loop method is proposed for identification of two-mass mechanical system. According to the authors' knowledge, indirect methods have not been applied in this context before (except in the preliminary study in [19]).[1]
2) The effect of the speed controller gain on identifiability is analyzed by means of simulations and experiments.
3) The proposed indirect identification method is experimentally compared with the open-loop identification method, the direct identification method, and the frequency-response based method proposed in [21].

II. MODEL OF A TWO-MASS MECHANICAL SYSTEM

The mechanical dynamics of the resonating two-mass system are given as [28]

$$J_{\mathrm{M}} \ddot{\theta}_{\mathrm{M}} = T_{\mathrm{M}} - T_{\mathrm{S}} - b_{\mathrm{M}} \dot{\theta}_{\mathrm{M}} \tag{1a}$$

$$J_{\mathrm{L}} \ddot{\theta}_{\mathrm{L}} = T_{\mathrm{S}} - T_{\mathrm{L}} - b_{\mathrm{L}} \dot{\theta}_{\mathrm{L}} \tag{1b}$$

$$T_{\mathrm{S}} = K_{\mathrm{S}}(\theta_{\mathrm{M}} - \theta_{\mathrm{L}}) + c_{\mathrm{S}}(\dot{\theta}_{\mathrm{M}} - \dot{\theta}_{\mathrm{L}}) \tag{1c}$$

where the angular positions of the motor and the load are θ_{M} and θ_{L}, respectively. The motor electromagnetic torque, the loading torque, and the shaft torque are T_{M}, T_{L}, and T_{S}, respectively. The motor speed is denoted by $\omega_{\mathrm{M}} = \dot{\theta}_{\mathrm{M}}$ and the load speed by $\omega_{\mathrm{L}} = \dot{\theta}_{\mathrm{L}}$. The moments of inertias of the motor and the load are denoted by J_{M} and J_{L}, respectively. The torsional stiffness and the damping of the shaft are K_{S} and c_{S}, respectively. The friction is modeled as viscous damping both on the motor and load sides, denoted by b_{M} and b_{L}, respectively. From (1), the open-loop transfer function from the torque $T_{\mathrm{M}}(s)$ to the speed $\omega_{\mathrm{M}}(s)$ is obtained as

$$G(s) = \frac{B(s)}{A(s)} \tag{2}$$

where

$$B(s) = J_{\mathrm{L}} s^2 + (c_{\mathrm{S}} + b_{\mathrm{L}}) s + K_{\mathrm{S}}$$

$$A(s) = J_{\mathrm{M}} J_{\mathrm{L}} s^3 + (J_{\mathrm{M}} c_{\mathrm{S}} + J_{\mathrm{L}} c_{\mathrm{S}} + J_{\mathrm{L}} b_{\mathrm{M}} + J_{\mathrm{M}} b_{\mathrm{L}}) s^2$$
$$+ (J_{\mathrm{M}} K_{\mathrm{S}} + J_{\mathrm{L}} K_{\mathrm{S}} + c_{\mathrm{S}} b_{\mathrm{M}} + c_{\mathrm{S}} b_{\mathrm{L}} + b_{\mathrm{M}} b_{\mathrm{L}}) s$$
$$+ K_{\mathrm{S}}(b_{\mathrm{M}} + b_{\mathrm{L}}).$$

[1]The main differences between this paper and the preliminary study are: 1) the parameters of the OE model are estimated using a straightforward iterative method; 2) the continuous-time transfer function parameters are analytically derived from the discrete-time pulse-transfer function parameters; and 3) the method is applied to estimate the mechanical parameters of an experimental two-mass system, whereas a two-mass system emulator was used in [19].

If $b_{\mathrm{M}} = 0$, $b_{\mathrm{L}} = 0$, and $c_{\mathrm{S}} = 0$ are assumed, the antiresonance frequency and the resonance frequency are

$$f_{\mathrm{ares}} = \frac{1}{2\pi} \sqrt{\frac{K_{\mathrm{S}}}{J_{\mathrm{L}}}} \qquad f_{\mathrm{res}} = \frac{1}{2\pi} \sqrt{K_{\mathrm{S}} \frac{J_{\mathrm{M}} + J_{\mathrm{L}}}{J_{\mathrm{M}} J_{\mathrm{L}}}} \tag{3}$$

respectively. It is to be noted that, at frequencies well below the antiresonance frequency, the transfer function (2) can be approximated by

$$G(s) = \frac{1}{(J_{\mathrm{M}} + J_{\mathrm{L}})s}. \tag{4}$$

On the other hand, at frequencies well above the resonance frequency, the transfer function (2) can be approximated by

$$G(s) = \frac{1}{J_{\mathrm{M}} s}. \tag{5}$$

III. PARAMETER ESTIMATION

First, three different identification setups are introduced. Then, parameters of the continuous-time mechanical model are linked with parameters of the discrete-time OE model. Further, factors affecting the accuracy of the parameter estimation are discussed.

A. Identification Setups

Three identification setups shown in Fig. 1 are considered. The PRBS torque excitation is applied in all setups. Typical torque-control bandwidths in ac servo drives are from several hundred hertz up to a few kilohertz, while dominant resonance frequencies of mechanical systems are lower. Hence, the torque-control loop is usually significantly faster than the mechanical system. If the sampling frequency of the parameter estimation is set significantly below the torque-control bandwidth, the effect of torque control cannot be seen in the identification signals and thus it can be omitted. In this paper, ideal torque control is assumed, i.e., $T_{\mathrm{M}} = T_{\mathrm{M,ref}}$.

An open-loop setup is shown in Fig. 1(a). The open-loop transfer function (2) can be directly estimated from the excitation signal u and the output signal y, i.e., $y(s) = G(s)u(s)$. If the excitation signal has a zero average, identification will be performed in the vicinity of zero speed. In this case, friction phenomena are highly nonlinear and can cause bias to the parameter estimates. Open-loop identification could also be performed during an acceleration test or a deceleration test. In these cases, the trend of the speed signal should be removed. Similar open-loop setups have been studied in [18], [21].

Fig. 1(b) shows a direct closed-loop setup, where the excitation signal is superimposed on the torque reference obtained from the speed controller.[2] The identification procedure is similar to the open-loop case. However, the identification input signal u and the noise (not shown in the figure) are now correlated due to the speed controller, which may lead to biased

[2]An equivalent identification setup could be formed, if the excitation signal is superimposed on the speed reference and a proportional speed controller is used. In this case, the amplitude of the excitation signal would depend on the gain of the speed controller.
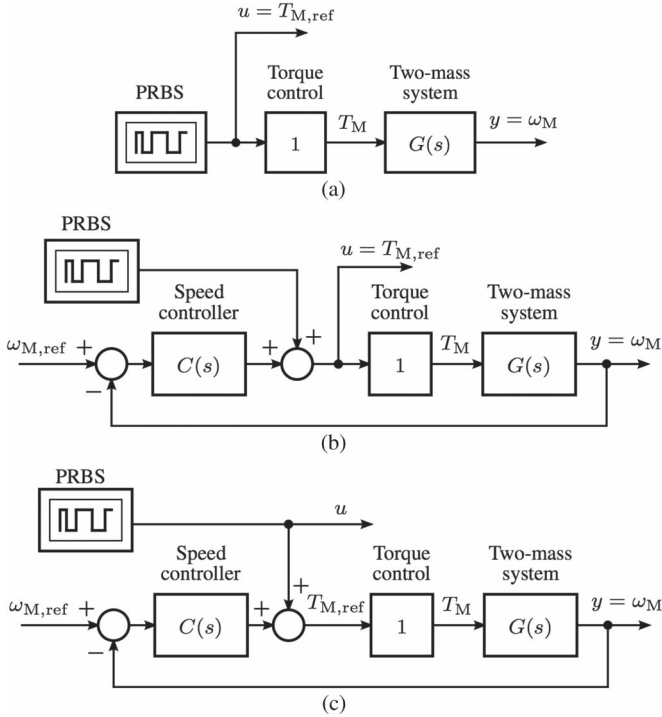
Fig. 1. Identification setups: (a) open loop; (b) direct closed loop; (c) indirect closed loop. Ideal torque control is assumed. Input and output identification signals are denoted by u and y, respectively.

parameter estimates. Similar direct setups have been considered in [18], [21].

Fig. 1(c) shows an indirect closed-loop identification setup. The excitation signal is superimposed on the torque reference as in the direct setup. The identification input signal u, however, is now the PRBS, which is not affected by the speed controller. The transfer function from the input $u(s)$ to the output $y(s)$ is

$$\frac{y(s)}{u(s)} = \frac{G(s)}{1 + G(s)C(s)}. \tag{6}$$

This closed-loop transfer function to be estimated contains the speed controller $C(s)$, whose effect on parameter estimates must be removed afterward. Therefore, the method is called indirect [29]. For simplicity, a proportional (P) speed controller is used, i.e., $C(s) = k_p$. Hence, the order of the transfer function to be identified is the same in all three setups. It is worth noticing that the indirect method can be applied for parameter estimation even if the speed controller output is not accessible (i.e., the direct closed-loop estimation method cannot be used), assuming that the speed controller gain is known *a priori*.

B. Mechanical Parameters

The discrete-time OE model applied in parameter estimation is

$$y(k) = \frac{B_d(z)}{A_d(z)} u(k) + e(k) \tag{7}$$

where z is the time-shift operator, $y(k)$ and $u(k)$ are the discrete samples corresponding to the signals y and u, respectively,

shown in Fig. 1, and $e(k)$ is the output noise in the system. The pulse-transfer function to be identified is given as

$$\frac{B_d(z)}{A_d(z)} = \frac{\theta_1 z^2 + \theta_2 z + \theta_3}{z^3 + \theta_4 z^2 + \theta_5 z + \theta_6} \tag{8}$$

where $\theta_1, \ldots, \theta_6$ are the six parameters to be estimated.

The output of the pulse-transfer function (8) can be expressed as

$$y(k) = \phi^T(k)\theta \tag{9}$$

where the regressor vector and the parameter vector are

$$\phi(k) = \begin{bmatrix} u(k-1) \\ u(k-2) \\ u(k-3) \\ -y(k-1) \\ -y(k-2) \\ -y(k-3) \end{bmatrix} \qquad \theta = \begin{bmatrix} \theta_1 \\ \theta_2 \\ \theta_3 \\ \theta_4 \\ \theta_5 \\ \theta_6 \end{bmatrix} \tag{10}$$

respectively. When the noise component is summed to the output of the system, solving the parameter vector using (9) and (10) leads to biased parameter estimates [29]. Here, a straightforward iterative method is applied to reduce the bias in the parameter estimates [30]. In this method, the input and output signals are filtered using the estimated system polynomial $\hat{A}_d(z)$ from the previous iteration. The output of the adaptive filtered system is given as

$$y_f(k) = \phi_f^T(k)\theta \tag{11}$$

where the filtered regressor vector and output are

$$\phi_f(k) = \frac{1}{\hat{A}_d(z)}\phi(k) \qquad y_f(k) = \frac{1}{\hat{A}_d(z)}y(k) \tag{12}$$

respectively. When estimating the parameter vector θ, the adaptive filtered output vector y_f and the regressor matrix Φ_f are given as

$$\Phi_f = \begin{bmatrix} \phi_f(3) & \phi_f(4) & \cdots & \phi_f(N) \end{bmatrix}^T$$
$$y_f = \begin{bmatrix} y_f(3) & y_f(4) & \cdots & y_f(N) \end{bmatrix}^T \tag{13}$$

where N is the total number of samples used in the parameter estimation. Then, the matrices are used in an iterative least-squares algorithm to solve the parameter vector

$$\theta = \left(\Phi_f^T \Phi_f\right)^{-1} \Phi_f^T y_f \tag{14}$$

which can be used to find $\hat{A}_d(z)$ for the next iteration

$$\hat{A}_d(z) = z^3 + \theta_4 z^2 + \theta_5 z + \theta_6. \tag{15}$$

During the first iteration, the filtering polynomial $\hat{A}_d(z) = 1$. The iterations are continued until the estimated parameters converge to the final values. It is important to check that the roots of $\hat{A}_d(z)$ are inside the unit circle after each iteration.

The pulse-transfer function (8) is then converted to a zero-pole matching equivalent continuous-time transfer function

$$\frac{y(s)}{u(s)} = \frac{b_1 s^2 + b_2 s + b_3}{s^3 + a_1 s^2 + a_2 s + a_3} \qquad (16)$$

where the parameters $b_1, \ldots, b_3$ and $a_1, \ldots, a_3$ are given in the Appendix. When comparing (6) and (16), the following system of equations is obtained:

$$b_1 = \frac{1}{J_M} \qquad b_2 = \frac{c_S + b_L}{J_M J_L} \qquad b_3 = \frac{K_S}{J_M J_L} \qquad (17a)$$

$$a_1 = \frac{(J_M + J_L)c_S + J_L b_M + J_M b_L + k_p J_L}{J_M J_L} \qquad (17b)$$

$$a_2 = \frac{(J_M + J_L)K_S + (b_M + b_L)c_S + b_M b_L + k_p(c_S + b_L)}{J_M J_L} \qquad (17c)$$

$$a_3 = \frac{K_S(b_M + b_L + k_p)}{J_M J_L}. \qquad (17d)$$

From (17), the mechanical parameters J_M, J_L, b_M, b_L, K_S, and c_S can be solved. In the open-loop and direct closed-loop identification setups, $k_p = 0$ is substituted into (17).

If the dominant resonance frequencies of the mechanical system were near the bandwidth of the torque control, the parameter estimates from (17) would be biased. If the bandwidth of the torque control is known, the dynamics of the torque-control loop could be included in the identification setups shown in Fig. 1.

If the identified system is highly nonlinear, the linear identification methods presented in this paper could be augmented with methods that can estimate the nonlinear elements, such as backlash or friction [12], [16], [31]–[33]. If the nonlinearity can be parametrized in the state variables (e.g., Coulomb friction), it could be introduced in the regressor vector ϕ in (10) [16]. Moreover, if the load inertia and the coupling stiffness vary during the drive operation [34], the presented identification methods could be used to estimate the parameters of the mechanical system in various operating points, and then construct a look-up table of parameter values as a function of operating point. Alternatively, recursive methods could be used to estimate the parameters online [20], [30], instead of the iterative method discussed above.

The presented methods are primarily aimed at identifying two-mass systems, i.e., the order of the discrete-time transfer function (8) is fixed. In the case of three-mass (or multi-mass) systems, the regressor and parameter vectors in (10) could be augmented and the parameters of the discrete-time transfer function estimated, but it is generally difficult to solve the relations between the discrete-time transfer-function coefficients and the physical parameters. However, since the resonances in typical multi-mass systems appear clearly at separate frequencies and the amplitude of the dominant low-frequency resonance is highest [18], [26], [34], the presented methods could be applied to identify the reduced-order (i.e., third-order) approximate model for multi-mass systems.

C. Sampling Frequency and the Number of Samples

According to the Nyquist-Shannon sampling theorem, the sampling frequency h of the discrete-time system should be at least twice the highest frequency in the original continuous-time signal. In most cases, the system response should also be modeled slightly above the resonance frequency to see if there are some additional dynamics at higher frequencies. However, if the sampling frequency is selected too high, numerical sensitivity issues can appear and cause the loss of identifiability. A high sampling frequency also causes the model fit to concentrate at high frequencies. A rule of thumb is to select the sampling frequency ten times the bandwidth of the process [29]. If a too low sampling frequency is selected, the higher frequencies of the system are not identified correctly, which further causes bias to the motor-side inertia estimate J_M according to (5).

If the model structure is chosen correctly, increasing the number of samples N should decrease the effect of disturbance noise and enhance the accuracy of parameter estimates. Memory and processing capacity may limit the number of samples. A rule of thumb for selecting the number of samples is $N = 1/(f_0 h)$, where f_0 is the lowest frequency to be identified and it should be much below the lowest potential antiresonance frequency. If too few samples are collected, lower frequencies of the system are not identified accurately, which further causes bias to the sum $J_M + J_L$ of the inertia estimates according to (4).

D. Model Validation

Model validation is an essential part of the identification procedure. The designer needs to know whether the selected model structure and the identification setup offers good enough information from the real system. A common tool in validation is residual analysis. Residual analysis is based on the statistical properties of the residuals $\varepsilon(k) = y(k) - \hat{y}(k)$. The simulated-system output is denoted as $\hat{y}(k) = G_d(z)u(k)$, where $G_d(z)$ represents the zero-pole equivalent discretization of the continuous-time time transfer function (2), which is obtained using the estimated system parameters.

The autocorrelation of the residuals is

$$R_\varepsilon(\tau) = \frac{1}{N} \sum_{k=1}^{N} \varepsilon(k)\varepsilon(k - \tau) \qquad (18)$$

where τ is the number of lags. The autocorrelation should ideally resemble that of white noise. Furthermore, the normalized cross-correlation

$$R_{\varepsilon,u}(\tau) = \frac{\sum_{k=1}^{N} \varepsilon(k)u(k - \tau)}{\sqrt{\sum_{k=1}^{N} \varepsilon^2(k) \sum_{k=1}^{N} u^2(k)}} \qquad (19)$$

between the input signal and the residuals should ideally be zero [30]. For the OE model, the emphasis in the residual analysis is in the cross-correlation since a noise model is not included in the OE structure [35]. Residual analysis should include large enough values of τ to cover frequencies down to the potential antiresonance frequency, i.e., $\tau h > 1/f_{\text{ares}}$. If
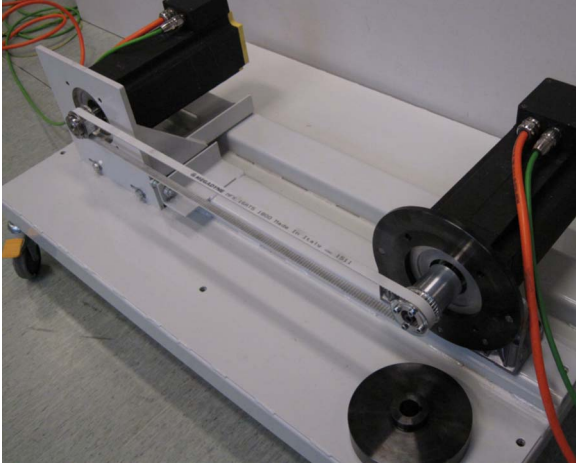
Fig. 2. Experimental setup.

possible, the residual analysis should be performed using a different input-output data set than the one which is used for the parameter estimation. Moreover, the identified model can be validated through the comparison of time- and frequency-domain responses of the identified and the measured (real) systems.

IV. RESULTS

The identification methods described in Section III are evaluated by means of simulations and experiments. First, the effect of the speed controller gain on the parameter estimates is studied by means of simulations. Then, the mechanical parameters of the experimental system are estimated and compared with the parameter estimates obtained using a frequency-response based identification method proposed in [21]. Finally, the results are validated using correlation and frequency-domain analyses.

A. Experimental System

The experimental setup is shown in Fig. 2. The setup consists of two mechanically coupled permanent-magnet synchronous motors (PMSMs). An inverter-fed 4-kW 2400-rpm PMSM, controlled with a dSPACE DS1104 board, is used as a driving motor. The driving motor is connected to a 4-kW loading servo motor using a flexible toothed belt. To vary coupling stiffness, different belts can be used. An additional inertia disk can be added to the shaft of the load motor.

The experiments were carried out using two mechanical configurations, referred to as Configurations A and B. The load-side inertia equals the motor-side inertia in Configuration A, while Configuration B has an additional inertia disk (increasing the load-side inertia). Furthermore, Configuration B has a stiffer belt.

Mechanical parameters were calculated based on the datasheet values of mechanical components [36]. These parameters are given in Tables I and II for Configurations A and B, respectively. The antiresonance and resonance frequencies of Configuration A, calculated using (3) with the datasheet values, are close to each other ($f_{ares} = 60$ Hz and $f_{res} = 84$ Hz), while the antiresonance and resonance frequencies of Configuration B

are far away from each other ($f_{ares} = 27$ Hz and $f_{res} = 79$ Hz). The datasheet values for c_S were approximated using

$$c_S = \frac{K_S}{2\pi f_{res} Q_k} \tag{20}$$

where $Q_k = 10$ was used for flexible couplings [37].

Torque control is accomplished through field-oriented control. The torque-control loop operates at 10-kHz sampling frequency and the torque-control bandwidth is 350 Hz. The speed-control loop operates at 1-kHz sampling frequency. The sampling frequency of the parameter estimation is 333 Hz, and the torque-control loop is ignored in parameter estimation. The number of samples is $N = 1620$. The excitation signal is a PRBS with values -2 Nm and 2 Nm (the rated torque being 17 Nm).

The rotor speed ω_M of the driving motor is measured using an incremental encoder. The angular speed is calculated from the measured angular position difference within the fixed sampling interval of 1 ms. This sampling scheme leads to a significant quantization noise especially at low rotational speeds which also favors the use of the OE model structure in the identification.

B. Benchmark Method for Experimental Comparison

The identification methods described in Section III are experimentally compared with a frequency-response based open-loop method proposed in [21]. The identification setup shown in Fig. 1(a) is applied. The experimental frequency-response function $G_e(j\omega)$ is evaluated in $M = 166$ data points between the frequencies of 1 Hz and 166 Hz by means of the Welch method. Two different Hamming-window lengths (540 and 270) were tested. Then, the parameter values of the analytical frequency-response function $G(j\omega)$ [obtained from (2)] are varied, and the best fit is iteratively searched by minimizing the error function

$$J(\boldsymbol{\vartheta}) = \sum_{i=1}^{M} |G_e(j\omega_i) - G(j\omega_i, \boldsymbol{\vartheta})|^2 \tag{21}$$

where the parameter vector is $\boldsymbol{\vartheta} = [J_M, J_L, K_S, c_S, b_M, b_L]$. The initial values of the parameter vector, needed in the first iteration, are selected according to the datasheet values given in Tables I and II.

C. Simulation Results

The speed controller is a P controller. The effect of the speed controller gain k_p on the estimated antiresonance and resonance frequencies is examined by means of simulations. A white-noise signal with variance of 1 rad^2/s^2 is added to the simulated motor speed. Numerical values for the resonance frequencies are calculated using (3), based on the estimated system parameters.

Fig. 3 shows the estimated resonance and antiresonance frequencies as a function of the speed controller gain for both the configurations. The system resembles the open-loop

TABLE I
DATASHEET VALUES AND ESTIMATED MECHANICAL PARAMETERS FOR CONFIGURATION A

Parameter	Datasheet	Parameters estimated using (17)			Frequency-response method [21] in open loop	
		Open loop	Direct	Indirect	Window length 540	Window length 270
J_M (kgm²)	0.005	0.0058	0.0060	0.0058	0.0050	0.0044
J_L (kgm²)	0.005	0.0047	0.0044	0.0044	0.0040	0.0037
K_S (Nm/rad)	700	656	651	646	591	580
c_S (Nms/rad)	0.13	0.08	0.04	0.03	0.05	0.05
b_M (Nms/rad)	0	−0.01	−0.16	−0.15	−0.33	−0.67
b_L (Nms/rad)	0	0.03	0.17	0.16	0.34	0.67

TABLE II
DATASHEET VALUES AND ESTIMATED MECHANICAL PARAMETERS FOR CONFIGURATION B

| Parameter	Datasheet	Parameters estimated using (17)			Frequency-response method [21] in open loop	
		Open loop	Direct	Indirect	Window length 540	Window length 270
J_M (kgm²)	0.005	0.0074	0.0069	0.0066	0.0057	0.0059
J_L (kgm²)	0.038	0.049	0.045	0.039	0.032	0.025
K_S (Nm/rad)	1100	1495	1414	1374	1231	1153
c_S (Nms/rad)	0.22	1.14	1.27	1.12	1.68	1.00
b_M (Nms/rad)	0	−1.28	−1.50	−1.39	−2.12	−1.36
b_L (Nms/rad)	0	1.30	1.58	1.40	2.12	1.36
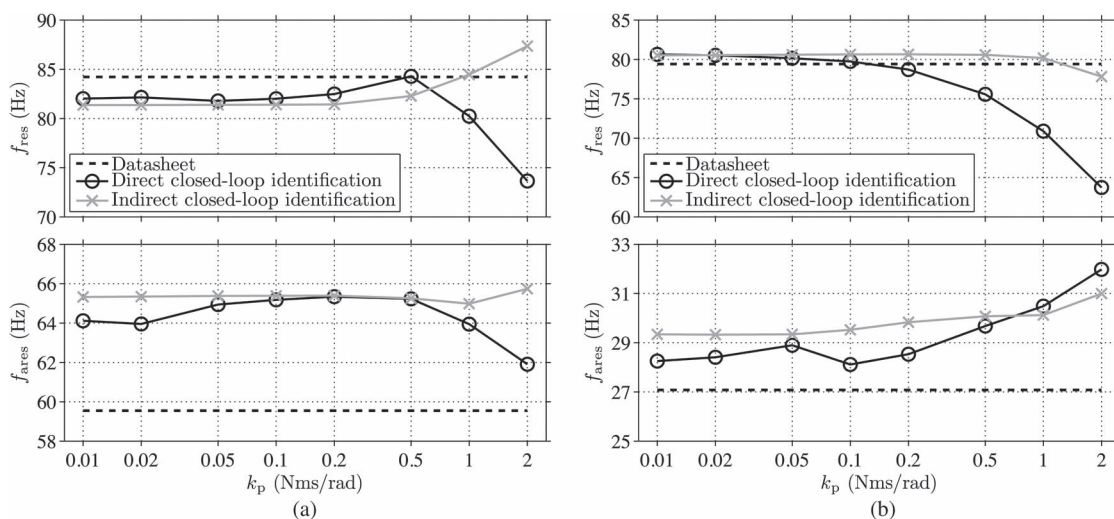
Fig. 3. Estimated resonance and antiresonance frequencies as a function of the speed controller gain: (a) Configuration A. (b) Configuration B. The results are obtained from simulations.

setup at low gain values ($k_\mathrm{p} < 0.1$ Nms/rad). In both closed-loop setups, high controller gains increase the effect of the measurement noise due to the feedback. The high controller gains ($k_\mathrm{p} > 1$ Nms/rad) also speed up the system, in which case the sampling frequency should be increased. This can be seen as biased resonance frequency estimates. It can be seen that the proposed indirect method is less sensitive to the selection of the speed controller gain than the direct method.

D. Experimental Results

In the closed-loop identification setups, the speed controller gain $k_\mathrm{p} = 0.2$ Nms/rad is selected and the parameters are estimated at the rotational speed of 200 r/min. To operate approximately at the speed of 200 r/min also in the open-loop setup, a constant offset torque is applied. The offset values are removed both from the input and output signals before

identification. For model validation, a separate input-output data set is measured in closed loop using the speed controller gain of $k_\mathrm{p} = 0.05$ Nms/rad.

The parameter estimates of Configurations A and B are given in Tables I and II, respectively. It can be seen that the parameter values estimated using (17) are close to those obtained using datasheets. However, it is important to notice that the datasheet-based parameter values are not necessarily more accurate than the estimated ones. Thus, also the datasheet-based parameter estimates shall be validated by means of residual analysis. In all the cases, an estimate of the motor-side damping b_M is negative. However, the sum $b_\mathrm{M} + b_\mathrm{L}$ of the viscous damping estimates is positive. Furthermore, when substituting the obtained parameter values back to the open-loop transfer function (2), all the coefficients of the transfer function are positive (i.e., the obtained poles and zeros are stable). When comparing the open-loop parameter estimates obtained using (17) with those of the
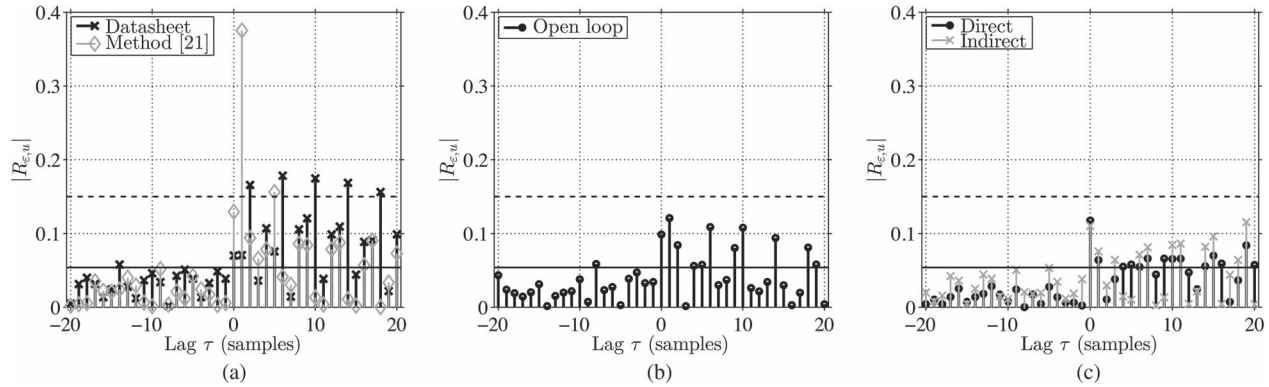
Fig. 4. Absolute values of normalized cross-correlation between input and residuals of Configuration A: (a) method [21] in open loop (Hamming-window length 540) and Datasheet values; (b) open loop; (c) closed loop. The 97% confidence limit is indicated as solid black line and the practical confidence limit as dashed black line.
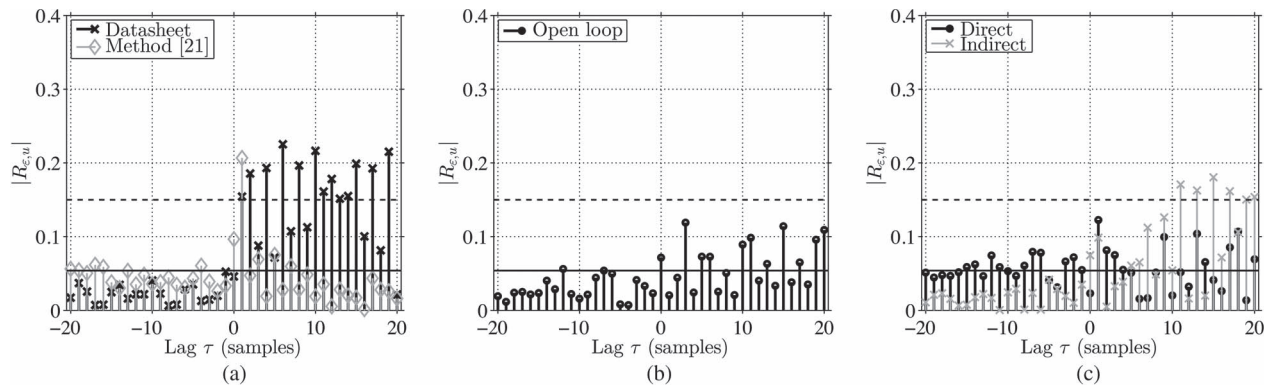

Fig. 5. Absolute values of normalized cross-correlation between input and residuals of Configuration B: (a) Method [21] in open loop (Hamming-window length 540) and Datasheet values; (b) open loop; (c) closed loop. The 97% confidence limit is indicated as solid black line and the practical confidence limit as dashed black line.

frequency-response method, it can be seen that the frequency-response method gives smaller values for the inertia moments and for the coupling stiffness. Moreover, Tables I and Table II show that the window length has a clear impact on the parameter estimates obtained using the frequency-response method.

The parameter estimates given in Tables I and II are first analyzed by means of residual analysis. The normalized cross correlation between the input signal and the residuals is evaluated using (19). Fig. 4 shows the cross-correlation absolute values for Configuration A and Fig. 5 for Configuration B. A 97% confidence limit (solid line) and a practical confidence limit (dashed line) are introduced in the figures [30]. The 97% confidence limit is calculated as $2.17/\sqrt{N}$, where N is the number of samples used in the estimation. Cross-correlation values remaining below the practical confidence limit will indicate that stochastically acceptable parameter estimates are obtained. It can be seen in Figs. 4(b) and (c), 5(b) and (c) that the normalized cross correlations between the input and the residuals remain mostly below the practical confidence limit in all the identification cases. Furthermore, the normalized cross-correlation values shown in Figs. 4(a) and (b), 5(a) and (b) indicate that the discrete-time polynomial-based identification method gives better parameter estimates than the frequency-response method [21] in an open-loop setup. The normalized

cross-correlation values shown in Figs. 4 and 5 also indicate that it is better to use the identified parameter values over the datasheet parameter values.

The frequency responses, obtained using the datasheet parameter values and the estimated parameter values, are compared. Fig. 6 shows the frequency responses of both the configurations obtained using the open-loop identification setups. It can be seen that the estimated amplitude is higher at lowest frequencies when the frequency-response method is applied because the inertia estimates are too low. When analyzing solely the locations of the antiresonance and resonance frequencies, it can be seen that the estimated resonance frequencies agree well with the datasheet-based resonance frequencies. In the case of the frequency-response method, the antiresonances appear at too high frequencies, because the load-inertia estimate is too low. These observations agree also with the numerical values given in Tables I and II. Fig. 7 shows the frequency responses of both the configurations obtained using the closed-loop identification setups. It can be seen that the estimated frequency responses agree well with the datasheet-based frequency responses. It should be noted that the estimated amplitudes at the resonance frequencies are not directly comparable with the datasheet-based amplitudes, because $b_{\mathrm{M}} = b_{\mathrm{L}} = 0$ are assumed in the case of datasheet values. Furthermore, the
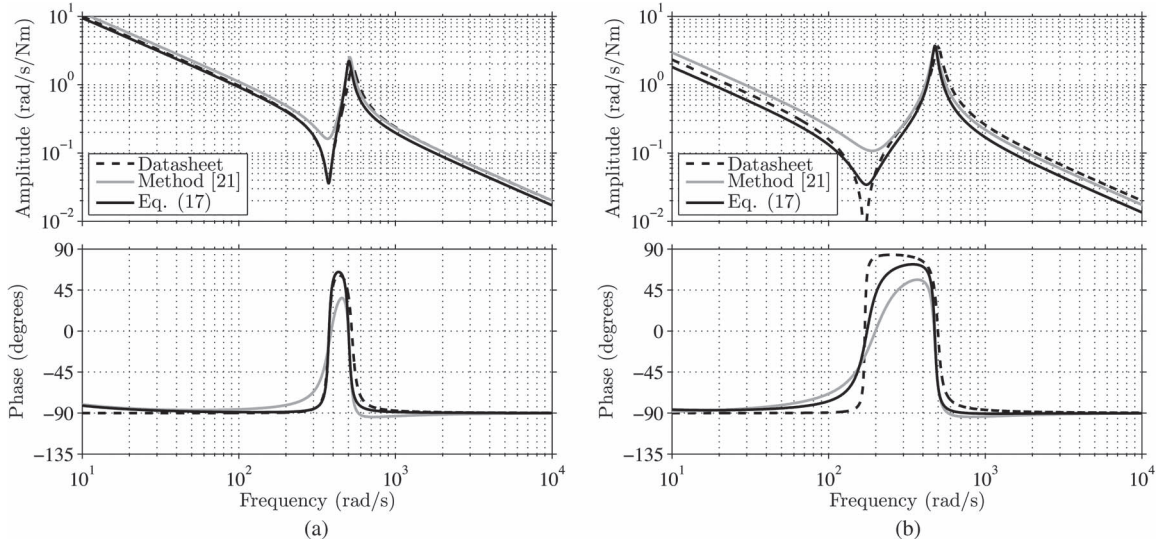
Fig. 6. Frequency responses obtained using open-loop identification method: (a) Configuration A. (b) Configuration B.
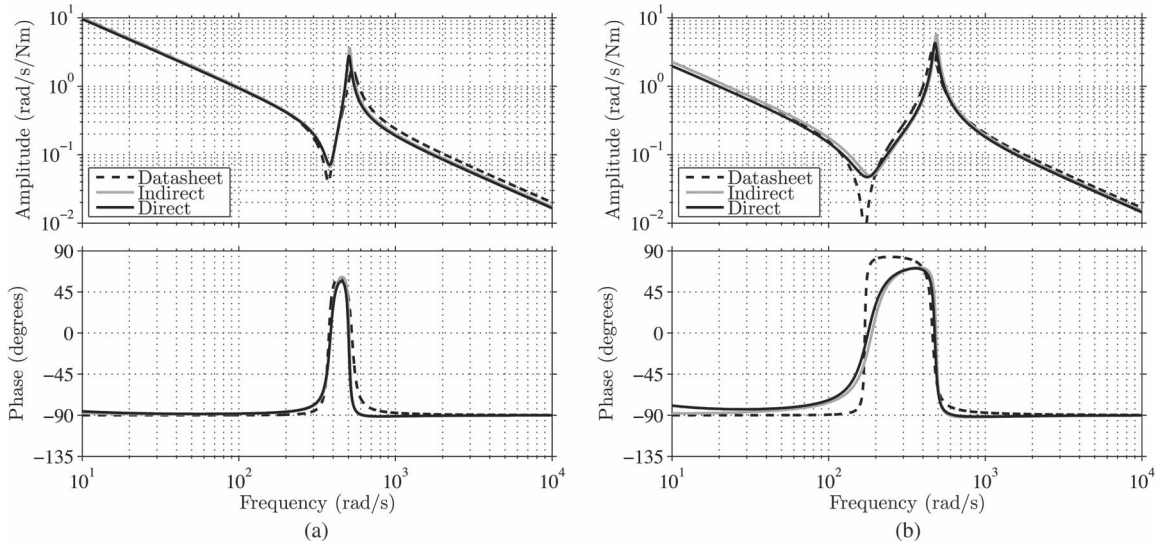

Fig. 7. Frequency responses obtained using closed-loop identification methods: (a) Configuration A. (b) Configuration B.

datasheet values of c_S are only rough approximations, obtained using (20).

V. CONCLUSION

This paper proposes an indirect closed-loop method for identification of two-mass mechanical system. Based on the simulation results, the proposed method is less sensitive to the selection of the speed controller gain than the direct method (when the simple OE model structure is used). The proposed indirect identification method was experimentally compared with the open-loop identification method, the direct identification method, and the frequency-response method. Based on the validation results, it can be concluded that all the identification setups are applicable for the parameter estimation of two-mass mechanical systems. The most biased estimate was the sum

of the viscous friction coefficients, which is rarely needed in motion controller tuning.

APPENDIX
CONTINUOUS-TIME TRANSFER FUNCTION PARAMETERS

The denominator of the pulse-transfer function (8) can be expressed as a combination of the first-order pole and the second-order complex-conjugate poles

$$\frac{B_d(z)}{A_d(z)} = \frac{\theta_1(z^2 + \beta_2 z + \beta_3)}{(z + \alpha_1)(z^2 + \alpha_2 z + \alpha_3)} \quad (22)$$

where

$$\beta_2 = \theta_2/\theta_1 \qquad \beta_3 = \theta_3/\theta_1$$
$$\alpha_1 + \alpha_2 = \theta_4 \qquad \alpha_1\alpha_2 + \alpha_3 = \theta_5 \qquad \alpha_1\alpha_3 = \theta_6.$$

The pulse-transfer function (22) is converted to a continuous-time zero-pole matching equivalent transfer function using the relation $s = (1/h)\ln(z)$, where h is the sampling interval [38]. The transfer function

$$\frac{y(s)}{u(s)} = \frac{b_1'\left(s^2 + 2b_2's + {b_2'}^2 + {b_3'}^2\right)}{(s + a_1')\left(s^2 + 2a_2's + {a_2'}^2 + {a_3'}^2\right)} \tag{23}$$

is obtained, where the parameters are

$$b_2' = -\frac{1}{h}\ln\left(\sqrt{\beta_3}\right) \tag{24a}$$

$$b_3' = \frac{1}{h}\arctan\left(\sqrt{4\beta_3/\beta_2^2 - 1}\right) \tag{24b}$$

$$a_1' = -\frac{1}{h}\ln(-\alpha_1) \qquad a_2' = -\frac{1}{h}\ln\left(\sqrt{\alpha_3}\right) \tag{24c}$$

$$a_3' = \frac{1}{h}\arctan\left(\sqrt{4\alpha_3/\alpha_2^2 - 1}\right) \tag{24d}$$

$$b_1' = \frac{a_1'\beta_1(1 + \beta_2 + \beta_3)\left({a_2'}^2 + {a_3'}^2\right)}{(1 + \alpha_1 + \alpha_2 + \alpha_1\alpha_2 + \alpha_3 + \alpha_1\alpha_3)\left({b_2'}^2 + {b_3'}^2\right)}. \tag{24e}$$

Using (24), the parameters in (16) are given as

$$b_1 = b_1' \qquad b_2 = 2b_1'b_2' \qquad b_3 = b_1'\left({b_2'}^2 + {b_3'}^2\right) \tag{25a}$$

$$a_1 = a_1' + 2a_2' \qquad a_2 = 2a_1'a_2' + {a_2'}^2 + {a_3'}^2 \tag{25b}$$

$$a_3 = a_1'\left({a_2'}^2 + {a_3'}^2\right). \tag{25c}$$

REFERENCES

[1] K. Ohishi and R. Furusawa, "Actuators for motion control: Fine actuator force control for electric injection molding machines," *IEEE Ind. Electron. Mag.*, vol. 6, no. 1, pp. 4–13, Mar. 2012.

[2] C. Hu, B. Yao, and Q. Wang, "Coordinated adaptive robust contouring controller design for an industrial biaxial precision gantry," *IEEE/ASME Trans. Mechatronics*, vol. 15, no. 5, pp. 728–735, Oct. 2010.

[3] M. Östring, S. Gunnarsson, and M. Norrlöf, "Closed-loop identification of an industrial robot containing flexibilities," *Control Eng. Practice*, vol. 11, no. 3, pp. 291–300, Mar. 2003.

[4] S. N. Vukosavic and M. R. Stojic, "Suppression of torsional oscillations in a high-performance speed servo drive," *IEEE Trans. Ind. Electron.*, vol. 45, no. 1, pp. 108–117, Feb. 1998.

[5] L. Harnefors, S. E. Saarakkala, and M. Hinkkanen, "Speed control of electrical drives using classical control methods," *IEEE Trans. Ind. Appl.*, vol. 49, no. 2, pp. 889–898, Mar./Apr. 2013.

[6] H.-B. Beck and D. Turschner, "Commissioning of a state-controlled high-powered electrical drive using evolutionary algorithms," *IEEE/ASME Trans. Mechatron.*, vol. 6, no. 2, pp. 149–154, Jun. 2001.

[7] L. Peretti and M. Zigliotto, "Identification of mechanical load for electrical drives commissioning - labeling machine case study," in *Proc. IEEE EUROCON*, May 2009, pp. 797–803.

[8] F. Schutte, S. Beineke, A. Rolfsmeier, and H. Grotstollen, "Online identification of mechanical parameters using extended Kalman filters," in *Conf. Rec. IEEE IAS Annu. Meeting*, Oct. 1997, vol. 1, pp. 501–508.

[9] M. A. Valenzuela, J. M. Bentley, and R. D. Lorenz, "Dynamic online sensing of sheet modulus of elasticity," *IEEE Trans. Ind. Appl.*, vol. 46, no. 1, pp. 108–120, Jan./Feb. 2010.

[10] K. Szabat and T. Orlowska-Kowalska, "Application of the Kalman filters to the high-performance drive system with elastic coupling," *IEEE Trans. Ind. Electron.*, vol. 59, no. 11, pp. 4226–4235, Nov. 2012.

[11] M. Perdomo, M. Pacas, T. Eutebach, and J. Immel, "Sensitivity analysis of the identification of variable inertia with an extended kalman filter," in *Proc. IEEE IECON*, Nov. 2013, pp. 3102–3107.

[12] R. Garrido and A. Concha, "An algebraic recursive method for parameter identification of a servo model," *IEEE/ASME Trans. Mechatron.*, vol. 18, no. 5, pp. 1572–1580, Oct. 2013.

[13] H. Zoubek, S. Villwock, and M. Pacas, "Frequency response analysis for rolling-bearing damage diagnosis," *IEEE Trans. Ind. Electron.*, vol. 55, no. 12, pp. 4270–4276, Sep. 2008.

[14] C. M. Wolf, K. M. Hanson, R. D. Lorenz, and M. A. Valenzuela, "Using the traction drive as the sensor to evaluate and track deterioration in electrified vehicle gearboxes," *IEEE Trans. Ind. Appl.*, vol. 49, no. 6, pp. 2610–2618, Nov./Dec. 2013.

[15] K.-K. Huh, R. D. Lorenz, and N. J. Nagel, "Gear fault diagnostics integrated in the motion servo drive for electromechanical actuators," *IEEE Trans. Ind. Appl.*, vol. 48, no. 1, pp. 142–150, Jan./Feb. 2012.

[16] S. Beineke, F. Schütte, H. Wertz, and H. Grotstollen, "Comparison of parameter identification schemes for self-commissioning drive control of nonlinear two-mass systems," in *Conf. Rec. IEEE IAS Annu. Meeting*, New Orleans, LA, USA, Oct. 1997, vol. 1, pp. 493–500.

[17] Y. Guo, L. Huang, and M. Muramatsu, "Research on inertia identification and auto-tuning of speed controller for AC servo system," in *Proc. IEEE Power Convers. Conf.*, Osaka, Japan, Apr. 2002, vol. 2, pp. 896–901.

[18] I. Eker and M. Vural, "Experimental online identification of a three-mass mechanical system," in *Proc. IEEE CCA Conf.*, Istanbul, Turkey, Jun. 2003, vol. 1, pp. 60–65.

[19] S. E. Saarakkala, T. Leppinen, M. Hinkkanen, and J. Luomi, "Parameter estimation of two-mass mechanical loads in electric drives," in *Proc. Adv. Motion Control Workshop*, Sarajevo, Bosnia and Hertsegovina, Mar. 2012, pp. 1–6.

[20] N. Nevaranta *et al.*, "Recursive identification of linear tooth belt-drive system," in *Proc. EPE Conf.*, Lappeenranta, Finland, Aug. 2014, pp. 1–8.

[21] S. Villwock and M. Pacas, "Application of the Welch-method for the identification of two- and three-mass-systems," *IEEE Trans. Ind. Electron.*, vol. 55, no. 1, pp. 457–466, Jan. 2008.

[22] Y. Yoshioka and T. Hanamoto, "Estimation of a multimass system using the LWTLS and a coefficient diagram for vibration-controller design," *IEEE Trans. Ind. Appl.*, vol. 44, no. 2, pp. 566–574, Mar./Apr. 2008.

[23] D.-H. Lee, J. H. Lee, and J.-W. Ahn, "Mechanical vibration reduction control of two-mass permanent magnet synchronous motor using adaptive notch filter with fast Fourier transform analysis," *IET Proc.-Electr. Power Appl.*, vol. 6, no. 7, pp. 455–461, Aug. 2012.

[24] S.-M. Yang and S.-C. Wang, "The detection of resonance frequency in motion control systems," *IEEE Trans. Ind. Appl.*, vol. 50, no. 5, pp. 3423–3427, Sep./Oct. 2014.

[25] U. Forssell and L. Ljung, "Closed-loop identification revisited," *Automatica*, vol. 35, no. 7, pp. 1215–1241, Jul. 1999.

[26] I. D. Landau and A. Karimi, "An output error recursive algorithm for unbiased identification in closed loop," *Automatica*, vol. 33, no. 5, pp. 933–938, May 1997.

[27] S. Villwock *et al.*, "Influence of the power density spectrum of the excitation signal on the identification of drives," in *Proc. IEEE IECON*, Orlando, FL, USA, Nov. 2008, pp. 1252–1257.

[28] G. Ellis, *Control System Design Guide: A Practical Guide*, 3rd ed. San Diego, CA, USA: Elsevier, 2004.

[29] L. Ljung, *System Identification: Theory for the User*, 2nd ed. Troy, NY, USA: Prentice-Hall, 1999.

[30] I. D. Landau and G. Zito, *Digital Control Systems: Design, Identification and Implementation*, 1st ed. Berlin, Germany: Springer-Verlag, 2006.

[31] C. T. Johnson and R. D. Lorenz, "Experimental identification of friction and its compensation in precise, position controlled mechanisms," *IEEE Trans. Ind. Appl.*, vol. 28, no. 6, pp. 1392–1398, Nov./Dec. 1992.

[32] D.-H. Lee and J.-W. Ahn, "Dual speed control scheme of servo drive system for a nonlinear friction compensation," *IEEE Trans. Power Electron.*, vol. 23, no. 2, pp. 959–965, Mar. 2008.

[33] S. Villwock and M. Pacas, "Time-domain identification method for detecting mechanical backlash in electrical drives," *IEEE Trans. Ind. Electron.*, vol. 56, no. 2, pp. 568–573, Feb. 2009.

[34] M. Jokinen, S. Saarakkala, M. Niemela, R. Pollanen, and J. Pyrhonen, "Physical drawbacks of linear high-speed tooth belt drives," in *Proc. Int. SPEEDAM*, Ischia, Italy, Jun. 2008, pp. 872–877.

[35] L. Ljung, *System Identification Toolbox: User's Guide*. Natick, MA, USA: The MathWorks Inc., 2010.

[36] S. E. Saarakkala, Identification and speed control design of resonating mechanical systems in electric drives, D.Sc. dissertation, Aalto Univ., Espoo, Finland, 2014.

[37] A. Frei, A. Grgic, W. Heil, and A. Luzi, "Design of pump shaft trains having variable-speed electric motors," in *Proc. Int. Pump Symp.*, Houston, TX, USA, 1986, pp. 33–44.

[38] G. F. Franklin, J. D. Powell, and M. L. Workman, *Digital Control of Dynamic Systems*, 3rd ed. Menlo Park, CA, USA: Addison-Wesley, 1997.

Seppo E. Saarakkala received the M.Sc.(Eng.) degree from Lappeenranta University of Technology, Lappeenranta, Finland, in 2008 and the D.Sc.(Tech.) degree from Aalto University, Espoo, Finland, in 2014.

Since 2010, he has been with the School of Electrical Engineering, Aalto University, Espoo, Finland, where he is currently a Post-Doctoral Research Scientist. His main research interests include control systems and electric drives.

Marko Hinkkanen (M'06–SM'13) received the M.Sc.(Eng.) and D.Sc.(Tech.) degrees from Helsinki University of Technology, Espoo, Finland, in 2000 and 2004, respectively.

Since 2000, he has been with Helsinki University of Technology (part of Aalto University, Espoo, since 2010). He is currently an Assistant Professor (tenure track) with the Aalto University School of Electrical Engineering. His research interests include control systems, electric drives, and power converters.